

AERIAL SPECTRUM SURVEYING: RADIO MAP ESTIMATION WITH AUTONOMOUS UAVS

Daniel Romero¹, Raju Shrestha¹, Yves Teganya¹, and Sundeep Prabhakar Chepuri²

¹Department of Information and Communication Technology, University of Agder, Norway.

²Department of Electrical Communication Engineering, Indian Institute of Science, India.

ABSTRACT

Radio maps are emerging as a popular means to endow next-generation wireless communications with situational awareness. In particular, radio maps are expected to play a central role in unmanned aerial vehicle (UAV) communications since they can be used to determine interference or channel gain at a spatial location where a UAV has not been before. Existing methods for radio map estimation utilize measurements collected by sensors whose locations cannot be controlled. In contrast, this paper proposes a scheme in which a UAV collects measurements along a trajectory. This trajectory is designed to obtain accurate estimates of the target radio map in a short time operation. The route planning algorithm relies on a map uncertainty metric to collect measurements at those locations where they are more informative. An online Bayesian learning algorithm is developed to update the map estimate and uncertainty metric every time a new measurement is collected, which enables real-time operation.

Index Terms— Radio maps, UAV communications, online estimation, route planning, active learning.

1. INTRODUCTION

Radio maps find a myriad of applications in wireless communications, such as network planning, interference coordination, power control, spectrum management, resource allocation, handoff procedure design, dynamic spectrum access, and cognitive radio; see e.g. [1, 2]. Recently, radio maps have received great attention for autonomous UAV communications and operations; see e.g. [3, 4]. These observations call for the development of a technology for “surveying” a spatial region of interest to construct a radio map. The goal of this paper is to address this task by collecting measurements with an autonomous UAV.

Over the last few years, a significant body of literature has addressed the estimation of radio maps from measurements acquired by spatially distributed sensors, typically by some form of interpolation algorithm. This includes kriging [5],

compressed sensing [6, 7], dictionary learning [8], matrix [9] and tensor completion [10], Bayesian models [11], kernel methods [12–14], thin-plate spline regression [15], and deep learning [16, 17]. In the context of UAV communications, radio map estimators have been proposed in [18]. All these schemes assume that the measurement positions are given and, hence, cannot decide where to measure next. Another related scheme is the one in [19], which does decide the trajectory of a UAV. However, the criterion is to minimize an outage metric and, thus, not tailored to construct a radio map.

This paper fills this gap by proposing *aerial spectrum surveying*, whereby a UAV autonomously collects measurements across the area of interest and adaptively decides where to measure next so that the time required to attain a prescribed estimation accuracy is approximately minimized.¹ To this end, the following challenges are addressed: (i) Since there are infinitely many candidate measurement locations in 3D space, the UAV needs to judiciously select an informative finite subset of them. To this end, a Bayesian learning scheme is adopted to estimate the radio map along with its uncertainty across space. Since adaptively planning the trajectory requires updating this uncertainty metric as more measurements are collected, an online learning algorithm with constant complexity per measurement is developed. (ii) Given the aforementioned metric, the UAV needs to plan a trajectory that prioritizes those points with a high uncertainty. To cope with the combinatorial complexity involved in this kind of formulations, two approximations are explored. The first relies on a receding horizon formulation cast as a *discounted-reward* travelling salesman problem, for which polynomial complexity approximations exist [20]. Since this complexity may still be unaffordable for real-time operation on board an UAV, a simpler waypoint-search scheme based on a shortest-path subroutine and a suitably designed spatial cost matrix is devised. This approach provides measurement locations at a low complexity while accounting for uncertainty and experience. The price to be paid is an increased suboptimality.

Sec. 2 addresses the contributions in (i) whereas Sec. 3 addresses those in (ii). The proposed scheme is validated

Research funded by the Research Council of Norway (IKTPLUS grant 280835) and the Indian Department of Science and Technology. {daniel.romero,raju.shrestha,yves.teganya}@uia.no, spchepuri@iisc.ac.in.

¹Although the focus is on UAVs, most of the ideas here can be extended to other mobile robots such as terrestrial vehicles.

through simulations in Sec. 4.

Notation: Boldface lowercase (uppercase) denote column vectors (matrices). For a random vector \mathbf{x} , notation $\mathcal{N}(\mathbf{x}|\boldsymbol{\mu}, \mathbf{C})$ or, its short-handed version $\mathcal{N}(\boldsymbol{\mu}, \mathbf{C})$, denotes a Gaussian distribution with mean $\boldsymbol{\mu}$ and covariance matrix \mathbf{C} .

2. ONLINE RADIO MAP LEARNING

After presenting the model, this section formulates the problems of estimating *power* and *service maps* as well as their associated uncertainty.

2.1. Radio Map Model

Let $\mathcal{X} \subset \mathbb{R}^d$ represent the geographical region of interest, where d is either 2 or 3, and consider a transmitter at location $\mathbf{x}_{\text{Tx}} \in \mathcal{X}$. This transmitter may correspond to a cellular base station. The location \mathbf{x}_{Tx} as well as the transmit power P_{Tx} can be assumed known as base stations in contemporary cellular networks share this information with the users. A single transmitter is assumed to keep the notation simple, but multiple transmitters can be readily accommodated. As usual, the power received at $\mathbf{x} \in \mathcal{X}$ is given in logarithmic units by

$$r(\mathbf{x}) = P_{\text{Tx}} + \bar{l}(\mathbf{x}) - \bar{s}(\mathbf{x}) + w(\mathbf{x}) \quad (1)$$

where each term is explained next. $\bar{l}(\mathbf{x})$ captures free-space path loss and antenna gain. $\bar{s}(\mathbf{x})$ is the shadowing loss, which captures attenuation due to obstructions. With the usual log-normal assumption, let $\bar{s}(\mathbf{x}) \sim \mathcal{N}(\mu_{\bar{s}}, \sigma_{\bar{s}}^2)$. Following the empirical model in [21], $\text{Cov}(\bar{s}(\mathbf{x}), \bar{s}(\mathbf{x}')) = c(\|\mathbf{x} - \mathbf{x}'\|)$, where function c is reparameterized here as $c(\delta) = \sigma_{\bar{s}}^2 2^{-\delta/\delta_0}$ with δ_0 the distance at which the correlation decays to 1/2. Finally, $w(\mathbf{x})$ accounts for small-scale fading, caused by the constructive/destructive interference between the signal paths arriving at \mathbf{x} , as well as additional unmodeled effects. As in [11], $w(\mathbf{x})$ will be modeled as $\mathcal{N}(0, \sigma_w^2)$. Additionally, it is assumed independent of $w(\mathbf{x}')$ and $\bar{s}(\mathbf{x}'')$ for all $\mathbf{x}', \mathbf{x}'' \in \mathcal{X}$ with $\mathbf{x}' \neq \mathbf{x}$. For clarity, rewrite (1) as

$$r(\mathbf{x}) = l(\mathbf{x}) - s(\mathbf{x}) + w(\mathbf{x}), \quad (2)$$

where $l(\mathbf{x}) \triangleq P_{\text{Tx}} + \bar{l}(\mathbf{x}) - \mu_{\bar{s}}$ and $s(\mathbf{x}) \triangleq \bar{s}(\mathbf{x}) - \mu_{\bar{s}}$. The deterministic component $l(\mathbf{x})$ can be assumed known as $\mu_{\bar{s}}$ can be readily estimated from a set of measurements.

To estimate the radio map, a UAV equipped with a communication module capable of measuring power and a GPS sensor collects measurements $(\mathbf{x}_\tau, \tilde{r}_\tau)$, $\tau = 0, 1, \dots$, where $\tilde{r}_\tau \triangleq r(\mathbf{x}_\tau) + z_\tau$ is the *received signal strength* at $\mathbf{x}_\tau \in \mathcal{X}$ and $z_\tau \sim \mathcal{N}(0, \sigma_z^2)$ models the measurement error, assumed independent across τ and independent of $w(\mathbf{x})$ and $s(\mathbf{x}')$ for all $\mathbf{x}, \mathbf{x}' \in \mathcal{X}$. The measurements and their locations up to and including time t will be arranged as $\tilde{\mathbf{r}}_t \triangleq [\tilde{r}_0, \dots, \tilde{r}_t]^\top \in \mathbb{R}^{t+1}$ and $\mathbf{X}_t \triangleq [\mathbf{x}_0, \dots, \mathbf{x}_t] \in \mathbb{R}^{d \times (t+1)}$.

2.2. Estimation Problem Formulation

This section formulates the problem of estimating two classes of radio maps given a collection of measurements.

Power Map Estimation. Given the above model, the *power map* $r(\mathbf{x})$ can be estimated with a conventional Gaussian-process estimator [22, Sec. 6.4]. Unfortunately, such *non-parametric* approaches incur unbounded complexity as their estimates involve the summation of one term per data point. To circumvent this effect, a key idea here is to aggregate the information provided by all the measurements up to and including time t by the posterior of $r(\mathbf{x})$ at a finite set of arbitrary grid points $\mathcal{G} \triangleq \{\mathbf{x}_0^g, \dots, \mathbf{x}_{G-1}^g\} \subset \mathcal{X}$. At these points, let (cf. (2))

$$\mathbf{r}^g \triangleq [r(\mathbf{x}_0^g), \dots, r(\mathbf{x}_{G-1}^g)]^\top = \mathbf{l}^g - \mathbf{s}^g + \mathbf{w}^g \quad (3)$$

where $\mathbf{l}^g \triangleq [l(\mathbf{x}_0^g), \dots, l(\mathbf{x}_{G-1}^g)]^\top$, $\mathbf{s}^g \triangleq [s(\mathbf{x}_0^g), \dots, s(\mathbf{x}_{G-1}^g)]^\top$, and $\mathbf{w}^g \triangleq [w(\mathbf{x}_0^g), \dots, w(\mathbf{x}_{G-1}^g)]^\top$. The *batch* version of the problem is to obtain $p(\mathbf{r}^g | \tilde{\mathbf{r}}_t, \mathbf{X}_t)$ given $\tilde{\mathbf{r}}_t$ and \mathbf{X}_t . One can then retrieve an estimate of \mathbf{r}^g as the mean of this posterior and an uncertainty metric from the covariance. However, given the unbounded complexity that such a task may entail, it is more convenient to address the *online* problem of iteratively finding $p(\mathbf{r}^g | \tilde{\mathbf{r}}_t, \mathbf{X}_t)$ given the previous posterior $p(\mathbf{r}^g | \tilde{\mathbf{r}}_{t-1}, \mathbf{X}_{t-1})$ and the most recent measurement $(\mathbf{x}_t, \tilde{r}_t)$ with bounded complexity per t .

Service Map Estimation. In UAV applications, rather than knowing the exact value of $r(\mathbf{x})$, it is often more relevant to know the set of locations \mathbf{x} that the base station can serve with a prescribed binary rate. This is necessary e.g. to establish a command-and-control channel or to communicate application-dependent data. Since the scheme can be readily extended to accommodate interference, assume for simplicity that the throughput is limited by noise and, therefore, one can regard location \mathbf{x} as served if $r(\mathbf{x}) \geq r_{\min}$ for a given r_{\min} . Let $\beta(\mathbf{x}) = 1$ in that case and $\beta(\mathbf{x}) = 0$ otherwise. The problem in this case is to find $p(\beta(\mathbf{x}_g^g) | \tilde{\mathbf{r}}_t, \mathbf{X}_t)$ for each g . The online and batch versions can be phrased as before.

2.3. Batch and Online Bayesian Estimators

Although the focus is on online learning, the solution to the batch problem is briefly described first to facilitate understanding. For notational convenience, let

$$\tilde{\mathbf{r}}_t = \mathbf{l}_t - \mathbf{s}_t + \mathbf{w}_t + \mathbf{z}_t, \quad (4)$$

where $\mathbf{l}_t \triangleq [l(\mathbf{x}_0), \dots, l(\mathbf{x}_t)]^\top$, $\mathbf{s}_t \triangleq [s(\mathbf{x}_0), \dots, s(\mathbf{x}_t)]^\top$, $\mathbf{w}_t \triangleq [w(\mathbf{x}_0), \dots, w(\mathbf{x}_t)]^\top$, and $\mathbf{z}_t \triangleq [z_0, \dots, z_t]^\top$.

Batch Power Map Estimator. From the model embodied by (3) and (4), it can be readily shown that \mathbf{r}^g is conditionally independent of $\tilde{\mathbf{r}}_t$ given \mathbf{s}^g . This, in turn, implies that

$$p(\mathbf{r}^g | \tilde{\mathbf{r}}_t) = \int p(\mathbf{r}^g | \mathbf{s}^g) p(\mathbf{s}^g | \tilde{\mathbf{r}}_t) d\mathbf{s}^g, \quad (5)$$

where \mathbf{X}_t has been omitted to lighten the notation. From (3) and the fact that $\mathbf{l}^{\mathcal{G}}$ is deterministic, it clearly follows that the first factor in the integrand is $p(\mathbf{r}^{\mathcal{G}}|\mathbf{s}^{\mathcal{G}}) = \mathcal{N}(\mathbf{r}^{\mathcal{G}}|\mathbf{l}^{\mathcal{G}} - \mathbf{s}^{\mathcal{G}}, \sigma_w^2 \mathbf{I}_G)$. To obtain the second factor $p(\mathbf{s}^{\mathcal{G}}|\tilde{\mathbf{r}}_t)$, observe that $\mathbf{s}^{\mathcal{G}}$ and $\tilde{\mathbf{r}}_t$ are jointly Gaussian. In particular, one can obtain the parameters of their joint distribution $p(\mathbf{s}^{\mathcal{G}}, \tilde{\mathbf{r}}_t)$ as follows. First, the mean vectors are clearly $\mathbb{E}[\mathbf{s}^{\mathcal{G}}] = \mathbf{0}$ and $\mathbb{E}[\tilde{\mathbf{r}}_t] = \mathbf{l}_t$. For the covariance, let $\text{Cov}[\mathbf{s}^{\mathcal{G}}] \triangleq \mathbf{C}_{\mathbf{s}^{\mathcal{G}}}$ and write $\text{Cov}[\mathbf{s}^{\mathcal{G}}, \tilde{\mathbf{r}}_t] = \mathbb{E}[\mathbf{s}^{\mathcal{G}}(\tilde{\mathbf{r}}_t - \mathbf{l}_t)^\top] = \mathbb{E}[\mathbf{s}^{\mathcal{G}}(-\mathbf{s}_t + \mathbf{w}_t + \mathbf{z}_t)^\top] = -\mathbb{E}[\mathbf{s}^{\mathcal{G}}\mathbf{s}_t^\top] \triangleq -\mathbf{C}_{\mathbf{s}^{\mathcal{G}}, \mathbf{s}_t}$ as well as $\text{Cov}[\tilde{\mathbf{r}}_t] = \mathbb{E}[(\tilde{\mathbf{r}}_t - \mathbf{l}_t)(\tilde{\mathbf{r}}_t - \mathbf{l}_t)^\top] = \mathbb{E}[(-\mathbf{s}_t + \mathbf{w}_t + \mathbf{z}_t)(-\mathbf{s}_t + \mathbf{w}_t + \mathbf{z}_t)^\top] = \text{Cov}[\mathbf{s}_t] + \sigma_w^2 \mathbf{I}_{t+1} + \sigma_z^2 \mathbf{I}_{t+1} \triangleq \mathbf{C}_{\mathbf{s}_t} + \sigma_w^2 \mathbf{I}_{t+1} + \sigma_z^2 \mathbf{I}_{t+1}$. Here, the matrices $\mathbf{C}_{\mathbf{s}^{\mathcal{G}}}$, $\mathbf{C}_{\mathbf{s}^{\mathcal{G}}, \mathbf{s}_t}$ and $\mathbf{C}_{\mathbf{s}_t}$ can be obtained from the covariance function c introduced in Sec. 2.1. Applying [23, Th. 10.2] to this joint distribution, it follows that $p(\mathbf{s}^{\mathcal{G}}|\tilde{\mathbf{r}}_t) = \mathcal{N}(\mathbf{s}^{\mathcal{G}}|\boldsymbol{\mu}_{\mathbf{s}^{\mathcal{G}}|\tilde{\mathbf{r}}_t}, \mathbf{C}_{\mathbf{s}^{\mathcal{G}}|\tilde{\mathbf{r}}_t})$, where

$$\begin{aligned} \boldsymbol{\mu}_{\mathbf{s}^{\mathcal{G}}|\tilde{\mathbf{r}}_t} &= \text{Cov}[\mathbf{s}^{\mathcal{G}}, \tilde{\mathbf{r}}_t] \text{Cov}^{-1}[\tilde{\mathbf{r}}_t](\tilde{\mathbf{r}}_t - \mathbb{E}[\tilde{\mathbf{r}}_t]) \\ &= -\mathbf{C}_{\mathbf{s}^{\mathcal{G}}, \mathbf{s}_t} (\mathbf{C}_{\mathbf{s}_t} + \sigma_w^2 \mathbf{I}_{t+1} + \sigma_z^2 \mathbf{I}_{t+1})^{-1} (\tilde{\mathbf{r}}_t - \mathbf{l}_t) \\ \mathbf{C}_{\mathbf{s}^{\mathcal{G}}|\tilde{\mathbf{r}}_t} &= \text{Cov}[\mathbf{s}^{\mathcal{G}}] - \text{Cov}[\mathbf{s}^{\mathcal{G}}, \tilde{\mathbf{r}}_t] \text{Cov}^{-1}[\tilde{\mathbf{r}}_t] \text{Cov}[\tilde{\mathbf{r}}_t, \mathbf{s}^{\mathcal{G}}] \\ &= \mathbf{C}_{\mathbf{s}^{\mathcal{G}}} - \mathbf{C}_{\mathbf{s}^{\mathcal{G}}, \mathbf{s}_t} (\mathbf{C}_{\mathbf{s}_t} + \sigma_w^2 \mathbf{I}_{t+1} + \sigma_z^2 \mathbf{I}_{t+1})^{-1} \mathbf{C}_{\mathbf{s}_t, \mathbf{s}^{\mathcal{G}}}, \end{aligned}$$

where $\mathbf{C}_{\mathbf{s}_t, \mathbf{s}^{\mathcal{G}}} \triangleq \mathbf{C}_{\mathbf{s}^{\mathcal{G}}, \mathbf{s}_t}^\top$. Finally, applying [22, eq. (2.115)] to obtain the conditional marginal (5) yields $p(\mathbf{r}^{\mathcal{G}}|\tilde{\mathbf{r}}_t) = \mathcal{N}(\mathbf{r}^{\mathcal{G}}|\boldsymbol{\mu}_{\mathbf{r}^{\mathcal{G}}|\tilde{\mathbf{r}}_t}, \mathbf{C}_{\mathbf{r}^{\mathcal{G}}|\tilde{\mathbf{r}}_t})$ with $\boldsymbol{\mu}_{\mathbf{r}^{\mathcal{G}}|\tilde{\mathbf{r}}_t} \triangleq \mathbf{l}_t - \boldsymbol{\mu}_{\mathbf{s}^{\mathcal{G}}|\tilde{\mathbf{r}}_t}$ and $\mathbf{C}_{\mathbf{r}^{\mathcal{G}}|\tilde{\mathbf{r}}_t} \triangleq \sigma_w^2 \mathbf{I}_G + \mathbf{C}_{\mathbf{s}^{\mathcal{G}}|\tilde{\mathbf{r}}_t}$, thereby solving the batch problem.

Online Power Map Estimator. To address the online power map estimation problem (see Sec. 2.2), it is convenient to decompose $p(\mathbf{r}^{\mathcal{G}}|\tilde{\mathbf{r}}_t)$ into $p(\mathbf{r}^{\mathcal{G}}|\tilde{\mathbf{r}}_{t-1})$ and a term that depends on the last measurement only. However, it can be easily seen that such a factorization is not possible due to the posterior correlation among measurements. To sidestep this difficulty, the central idea in the proposed online learning scheme (see also Sec. 2.2) is to use \mathcal{G} to summarize the information of all past measurements. Mathematically, this can be phrased as the assumption that $\tilde{\mathbf{r}}_t$ and $\tilde{\mathbf{r}}_{t-1}$ are conditionally independent given $\mathbf{r}^{\mathcal{G}}$. That is, when $\mathbf{r}^{\mathcal{G}}$ is known, the past measurements $\tilde{\mathbf{r}}_{t-1}$ do not provide extra information about $\tilde{\mathbf{r}}_t$. The error that this approximation introduces can be reduced by adopting a denser grid and pays off since it enables online estimation.

From this assumption and Bayes' rule, it follows that

$$\begin{aligned} p(\mathbf{r}^{\mathcal{G}}|\tilde{\mathbf{r}}_t) &= p(\mathbf{r}^{\mathcal{G}}|\tilde{\mathbf{r}}_t, \tilde{\mathbf{r}}_{t-1}) \propto p(\tilde{\mathbf{r}}_t, \tilde{\mathbf{r}}_{t-1}|\mathbf{r}^{\mathcal{G}}) p(\mathbf{r}^{\mathcal{G}}) \\ &= p(\tilde{\mathbf{r}}_t|\mathbf{r}^{\mathcal{G}}) p(\tilde{\mathbf{r}}_{t-1}|\mathbf{r}^{\mathcal{G}}) p(\mathbf{r}^{\mathcal{G}}) = p(\tilde{\mathbf{r}}_{t-1}, \mathbf{r}^{\mathcal{G}}) p(\tilde{\mathbf{r}}_t|\mathbf{r}^{\mathcal{G}}) \\ &= p(\mathbf{r}^{\mathcal{G}}|\tilde{\mathbf{r}}_{t-1}) p(\tilde{\mathbf{r}}_{t-1}|\mathbf{r}^{\mathcal{G}}) p(\tilde{\mathbf{r}}_t|\mathbf{r}^{\mathcal{G}}) \propto p(\mathbf{r}^{\mathcal{G}}|\tilde{\mathbf{r}}_{t-1}) p(\tilde{\mathbf{r}}_t|\mathbf{r}^{\mathcal{G}}), \end{aligned}$$

where \propto denotes equality up to a positive factor that does not depend on $\mathbf{r}^{\mathcal{G}}$. As shown earlier in this section, $p(\mathbf{r}^{\mathcal{G}}|\tilde{\mathbf{r}}_{t-1}) = \mathcal{N}(\mathbf{r}^{\mathcal{G}}|\boldsymbol{\mu}_{\mathbf{r}^{\mathcal{G}}|\tilde{\mathbf{r}}_{t-1}}, \mathbf{C}_{\mathbf{r}^{\mathcal{G}}|\tilde{\mathbf{r}}_{t-1}})$. Since $p(\mathbf{r}^{\mathcal{G}}|\tilde{\mathbf{r}}_{t-1})$ is given in the online formulation (cf. Sec. 2.2), the online learning algorithm can use $\boldsymbol{\mu}_{\mathbf{r}^{\mathcal{G}}|\tilde{\mathbf{r}}_{t-1}}$ and $\mathbf{C}_{\mathbf{r}^{\mathcal{G}}|\tilde{\mathbf{r}}_{t-1}}$ to obtain $p(\mathbf{r}^{\mathcal{G}}|\tilde{\mathbf{r}}_t)$.

To find $p(\tilde{\mathbf{r}}_t|\mathbf{r}^{\mathcal{G}})$, note that $\tilde{\mathbf{r}}_t$ and $\mathbf{r}^{\mathcal{G}}$ are jointly Gaussian. It follows from [23, Th. 10.2] that $p(\tilde{\mathbf{r}}_t|\mathbf{r}^{\mathcal{G}})$ is Gaussian dis-

tributed with parameters

$$\begin{aligned} \mathbb{E}[\tilde{\mathbf{r}}_t|\mathbf{r}^{\mathcal{G}}] &= \mathbb{E}[\tilde{\mathbf{r}}_t] + \text{Cov}[\tilde{\mathbf{r}}_t, \mathbf{r}^{\mathcal{G}}] \text{Cov}^{-1}[\mathbf{r}^{\mathcal{G}}](\mathbf{r}^{\mathcal{G}} - \mathbb{E}[\mathbf{r}^{\mathcal{G}}]) \\ &= \mathbf{l}(\mathbf{x}_t) + \mathbb{E}[(-\mathbf{s}(\mathbf{x}_t) + \mathbf{w}(\mathbf{x}_t) + \mathbf{z}_t)(-\mathbf{s}^{\mathcal{G}} + \mathbf{w}^{\mathcal{G}})^\top] \\ &\quad \times \mathbb{E}^{-1}[(-\mathbf{s}^{\mathcal{G}} + \mathbf{w}^{\mathcal{G}})(-\mathbf{s}^{\mathcal{G}} + \mathbf{w}^{\mathcal{G}})^\top](\mathbf{r}^{\mathcal{G}} - \mathbf{l}^{\mathcal{G}}) \\ &= \mathbf{l}(\mathbf{x}_t) + (\mathbf{C}_{\mathbf{s}(\mathbf{x}_t), \mathbf{s}^{\mathcal{G}}} + \mathbf{C}_{\mathbf{w}(\mathbf{x}_t), \mathbf{w}^{\mathcal{G}}}) \\ &\quad \times (\mathbf{C}_{\mathbf{s}^{\mathcal{G}}} + \sigma_w^2 \mathbf{I}_G)^{-1} (\mathbf{r}^{\mathcal{G}} - \mathbf{l}^{\mathcal{G}}) \triangleq \mathbf{a}_t^\top \mathbf{r}^{\mathcal{G}} + b_t \\ \text{Var}[\tilde{\mathbf{r}}_t|\mathbf{r}^{\mathcal{G}}] &= \text{Var}[\tilde{\mathbf{r}}_t] - \text{Cov}[\tilde{\mathbf{r}}_t, \mathbf{r}^{\mathcal{G}}] \text{Cov}^{-1}[\mathbf{r}^{\mathcal{G}}] \text{Cov}[\mathbf{r}^{\mathcal{G}}, \tilde{\mathbf{r}}_t] \\ &= \sigma_s^2 + \sigma_w^2 + \sigma_z^2 - (\mathbf{C}_{\mathbf{s}(\mathbf{x}_t), \mathbf{s}^{\mathcal{G}}} + \mathbf{C}_{\mathbf{w}(\mathbf{x}_t), \mathbf{w}^{\mathcal{G}}}) \\ &\quad \times (\mathbf{C}_{\mathbf{s}^{\mathcal{G}}} + \sigma_w^2 \mathbf{I}_G)^{-1} (\mathbf{C}_{\mathbf{s}(\mathbf{x}_t), \mathbf{s}^{\mathcal{G}}} + \mathbf{C}_{\mathbf{w}(\mathbf{x}_t), \mathbf{w}^{\mathcal{G}}})^\top \triangleq \lambda_t, \end{aligned}$$

where the quantities $\mathbf{a}_t \triangleq (\mathbf{C}_{\mathbf{s}^{\mathcal{G}}} + \sigma_w^2 \mathbf{I}_G)^{-1} (\mathbf{C}_{\mathbf{s}(\mathbf{x}_t), \mathbf{s}^{\mathcal{G}}} + \mathbf{C}_{\mathbf{w}(\mathbf{x}_t), \mathbf{w}^{\mathcal{G}}})^\top$ and $b_t \triangleq \mathbf{l}(\mathbf{x}_t) - (\mathbf{C}_{\mathbf{s}(\mathbf{x}_t), \mathbf{s}^{\mathcal{G}}} + \mathbf{C}_{\mathbf{w}(\mathbf{x}_t), \mathbf{w}^{\mathcal{G}}}) (\mathbf{C}_{\mathbf{s}^{\mathcal{G}}} + \sigma_w^2 \mathbf{I}_G)^{-1} \mathbf{l}^{\mathcal{G}}$ have been defined along with $\mathbf{C}_{\mathbf{s}(\mathbf{x}_t), \mathbf{s}^{\mathcal{G}}} \triangleq \text{Cov}[\mathbf{s}(\mathbf{x}_t), \mathbf{s}^{\mathcal{G}}]$ and $\mathbf{C}_{\mathbf{w}(\mathbf{x}_t), \mathbf{w}^{\mathcal{G}}} \triangleq \text{Cov}[\mathbf{w}(\mathbf{x}_t), \mathbf{w}^{\mathcal{G}}]$. Clearly, the latter contains a single non-zero entry if $\mathbf{x}_t \in \mathcal{G}$ and vanishes otherwise.

Finally, it follows from [22, eq. (2.116)] that the requested posterior is $p(\mathbf{r}^{\mathcal{G}}|\tilde{\mathbf{r}}_t) = \mathcal{N}(\mathbf{r}^{\mathcal{G}}|\boldsymbol{\mu}_{\mathbf{r}^{\mathcal{G}}|\tilde{\mathbf{r}}_t}, \mathbf{C}_{\mathbf{r}^{\mathcal{G}}|\tilde{\mathbf{r}}_t})$ with

$$\begin{aligned} \mathbf{C}_{\mathbf{r}^{\mathcal{G}}|\tilde{\mathbf{r}}_t} &= (\mathbf{C}_{\mathbf{r}^{\mathcal{G}}|\tilde{\mathbf{r}}_{t-1}}^{-1} + (1/\lambda_t) \mathbf{a}_t \mathbf{a}_t^\top)^{-1} \\ &= \mathbf{C}_{\mathbf{r}^{\mathcal{G}}|\tilde{\mathbf{r}}_{t-1}} - \frac{\mathbf{C}_{\mathbf{r}^{\mathcal{G}}|\tilde{\mathbf{r}}_{t-1}} \mathbf{a}_t \mathbf{a}_t^\top \mathbf{C}_{\mathbf{r}^{\mathcal{G}}|\tilde{\mathbf{r}}_{t-1}}}{\lambda_t + \mathbf{a}_t^\top \mathbf{C}_{\mathbf{r}^{\mathcal{G}}|\tilde{\mathbf{r}}_{t-1}} \mathbf{a}_t} \\ \boldsymbol{\mu}_{\mathbf{r}^{\mathcal{G}}|\tilde{\mathbf{r}}_t} &= \mathbf{C}_{\mathbf{r}^{\mathcal{G}}|\tilde{\mathbf{r}}_t} \left[\frac{\tilde{\mathbf{r}}(\mathbf{x}_t) - b_t}{\lambda_t} \mathbf{a}_t + \mathbf{C}_{\mathbf{r}^{\mathcal{G}}|\tilde{\mathbf{r}}_{t-1}}^{-1} \boldsymbol{\mu}_{\mathbf{r}^{\mathcal{G}}|\tilde{\mathbf{r}}_{t-1}} \right]. \end{aligned}$$

The sought algorithm applies these two update equations every time a new measurement is acquired. The initializations are given by $\mathbf{C}_{\mathbf{r}^{\mathcal{G}}|\tilde{\mathbf{r}}_{-1}} \triangleq \mathbf{C}_{\mathbf{s}^{\mathcal{G}}} + \sigma_w^2 \mathbf{I}_G$ and $\boldsymbol{\mu}_{\mathbf{r}^{\mathcal{G}}|\tilde{\mathbf{r}}_{-1}} \triangleq \mathbf{l}^{\mathcal{G}}$.

Service Map Estimation. Since the service map $\beta(\mathbf{x})$ is a function of $r(\mathbf{x})$, it is not surprising that the algorithm from the previous section can be readily extended to obtain service maps. To this end, apply Bayes rule and note that $\beta(\mathbf{x}_g^{\mathcal{G}})$ is deterministically solely determined by $r(\mathbf{x}_g^{\mathcal{G}})$ to write

$$\begin{aligned} p(\beta(\mathbf{x}_g^{\mathcal{G}})|\tilde{\mathbf{r}}_t) &= \int p(\beta(\mathbf{x}_g^{\mathcal{G}}), \mathbf{r}^{\mathcal{G}}|\tilde{\mathbf{r}}_t) d\mathbf{r}^{\mathcal{G}} \\ &= \int p(\beta(\mathbf{x}_g^{\mathcal{G}})|\mathbf{r}^{\mathcal{G}}, \tilde{\mathbf{r}}_t) p(\mathbf{r}^{\mathcal{G}}|\tilde{\mathbf{r}}_t) d\mathbf{r}^{\mathcal{G}} \\ &= \int p(\beta(\mathbf{x}_g^{\mathcal{G}})|r(\mathbf{x}_g^{\mathcal{G}})) p(\mathbf{r}^{\mathcal{G}}|\tilde{\mathbf{r}}_t) d\mathbf{r}^{\mathcal{G}} \\ &= \int p(\beta(\mathbf{x}_g^{\mathcal{G}})|r(\mathbf{x}_g^{\mathcal{G}})) p(r(\mathbf{x}_g^{\mathcal{G}})|\tilde{\mathbf{r}}_t) dr(\mathbf{x}_g^{\mathcal{G}}). \end{aligned}$$

Noting that $p(\beta(\mathbf{x}_g^{\mathcal{G}})|r(\mathbf{x}_g^{\mathcal{G}})) = 1$ if $r(\mathbf{x}_g^{\mathcal{G}}) \geq r_{\min}$ and 0 otherwise, the distribution of $\beta(\mathbf{x}_g^{\mathcal{G}})$ is fully characterized by

$$p_g^\beta \triangleq \mathbb{P}[\beta(\mathbf{x}_g^{\mathcal{G}}) = 1|\tilde{\mathbf{r}}_t] = \int_{r_{\min}}^{\infty} p(r(\mathbf{x}_g^{\mathcal{G}})|\tilde{\mathbf{r}}_t) dr(\mathbf{x}_g^{\mathcal{G}}). \quad (7)$$

The latter expression can be evaluated through the cumulative distribution function of a Gaussian random variable using the mean and variance of $p(r(\mathbf{x}_g^{\mathcal{G}})|\tilde{\mathbf{r}}_t)$ obtained earlier.

3. ADAPTIVE TRAJECTORY DESIGN

Since the UAV can navigate to arbitrary locations in \mathcal{X} to acquire measurements, the problem becomes how to design a trajectory such that this acquisition is performed as efficiently as possible. Since there is a trade-off between time and estimation performance, a more formal problem statement would be, as described later, to minimize the time required to obtain a map estimate with a prescribed accuracy. However, quantifying accuracy is itself a problem since the true map is not available to the UAV. For this reason, it is necessary to develop a suitable metric that the UAV can compute given the measurements and prior information.

3.1. Uncertainty Metric

The goal of this section is to design $u_g(\tilde{\mathbf{r}}_t) \in [0, 1]$, which denotes the uncertainty in the target (power or service) map at \mathbf{x}_g^G after observing $\tilde{\mathbf{r}}_t$. If the goal is to estimate a power map, it seems reasonable to use the posterior variance. To ensure that the resulting metric is in $[0, 1]$, one may normalize by the prior variance, since the latter constitutes an upper bound for the posterior variance. This yields

$$u_g(\tilde{\mathbf{r}}_t) = \frac{[C_{r^g|\tilde{\mathbf{r}}_t}]_{g,g}}{\sigma_s^2 + \sigma_w^2}. \quad (8)$$

In turn, for service map estimation, note that there is little uncertainty when $r(\mathbf{x})$ is known to be very large or very small: the most uncertain points are those where p_g^β is close to $1/2$. This is naturally quantified by the posterior entropy of $\beta(\mathbf{x}_g^G)$:

$$u_g(\tilde{\mathbf{r}}_t) = -p_g^\beta \log_2(p_g^\beta) - (1 - p_g^\beta) \log_2(1 - p_g^\beta). \quad (9)$$

When there are multiple transmitters, the values of the relevant metric (either (8) or (9)) for all transmitters can be aggregated (e.g. by averaging or taking the maximum) to obtain a single $u_g(\tilde{\mathbf{r}}_t)$ per g .

With these point-wise uncertainty metrics, one can quantify the total uncertainty of the map after observing $\tilde{\mathbf{r}}_t$ by the spatial average $u(\tilde{\mathbf{r}}_t) \triangleq (1/G) \sum_{g=0}^{G-1} u_g(\tilde{\mathbf{r}}_t)$.

3.2. Route Planning

The UAV may use past measurements as well as prior information about the map to decide where to measure next. Formally, $\mathbf{x}_{t+1} = \pi(\tilde{\mathbf{r}}_t, \mathbf{X}_t)$, where function π is the policy that needs to be designed. Informally, one would like that $u(\tilde{\mathbf{r}}_t)$ decreases as fast as possible over time. However, the specific criterion adopted to design π may depend on the user's preferences. Let $T(\mathbf{X}_t)$ denote the time that the UAV needs to follow the trajectory defined by the points in \mathbf{X}_t . A reasonable simplification is that the UAV moves at constant speed v and, therefore, $T(\mathbf{X}_t) = \sum_{\tau=1}^t \|\mathbf{x}_\tau - \mathbf{x}_{\tau-1}\|/v$. One may be, for example, interested in the π that minimizes

$\mathbb{E}[u(\tilde{\mathbf{r}}_t)]$, where t and \mathbf{X}_t are such that $T(\mathbf{X}_t)$ is below a given upper bound. Alternatively, one could minimize $\mathbb{E}[T(\mathbf{X}_t)]$ subject to an upper bound on $u(\tilde{\mathbf{r}}_t)$. Yet another possible criterion would be to maximize the discounted reward $\mathbb{E}[\sum_{\tau=1}^t \gamma^{T(\mathbf{X}_\tau)} (u(\tilde{\mathbf{r}}_{\tau-1}) - u(\tilde{\mathbf{r}}_\tau))]$ with $\gamma \in (0, 1)$ given. Clearly, this objective promotes trajectories with large uncertainty improvements $u(\tilde{\mathbf{r}}_{\tau-1}) - u(\tilde{\mathbf{r}}_\tau)$ at the beginning.

All these formulations lead to non-convex optimization problems where the optimization variable is the function π . Thus, it is necessary to discretize the set of candidate measurement locations, for instance by restricting $\mathbf{x}_t \in \mathcal{G}$. Unfortunately, even in that case, this kind of problems can be shown to be NP-hard; see e.g. [20, 24] and references therein. Thus, one needs to resort to approximations.

In the case of power maps, note that (8) does not depend on the measurements, but only on their location. Therefore, a (suboptimal) trajectory can be found in an offline fashion, for example along the lines of the algorithm in [24] and references therein. In turn, for service maps, the metric (9) does depend on the measurements and, therefore, the trajectory should be computed on-the-fly, as measurements are collected. However, updating the trajectory with the reception of every new measurement may be too costly. Besides, the presence of expectations in the aforementioned objectives renders such a task intractable. A more sensible alternative is to update the trajectory every t_{upd} measurements, assuming that $u_g(\tilde{\mathbf{r}}_t)$ remains approximately constant between consecutive updates at all grid points except where a measurement is collected, in which case $u_g(\tilde{\mathbf{r}}_t)$ becomes 0 at that point. In other words, measuring at location $\mathbf{x}_t = \mathbf{x}_g^G$ yields $u(\tilde{\mathbf{r}}_t) \approx u_g(\tilde{\mathbf{r}}_{t-1}) - (1/G)u_g(\tilde{\mathbf{r}}_{t-1})$.

Such a receding horizon approach could be cast as an instance of the so-called *weighted-reward traveling salesman problem* and a solution could be approximated by means of the algorithm in [20], which has a polynomial complexity. For real-time UAV operations, limited by computational power, it may be preferable to pursue alternatives with lower complexity, yet higher suboptimality. The alternative explored here is to select, at each trajectory update, a destination in \mathcal{G} with highest local uncertainty. For rectangular \mathcal{G} , if $u_g(\tilde{\mathbf{r}}_t)$ is organized as a matrix, this destination can be found as the maximum of such a matrix spatially filtered by a low-pass kernel. The route to reach that destination can be sought by minimizing the line integral of $u_{\mathbf{x}}(\tilde{\mathbf{r}}_t)$ along the trajectory, where $u_{\mathbf{x}}(\tilde{\mathbf{r}}_t)$ denotes the uncertainty at \mathbf{x} . This trajectory can be approximated through a shortest-path algorithm (e.g. Bellman-Ford) with edge cost between \mathbf{x}_g^G and $\mathbf{x}_{g'}^G$ given by the reciprocal of $\int_{\mathbf{x}_g^G}^{\mathbf{x}_{g'}^G} u_{\mathbf{x}}(\tilde{\mathbf{r}}_t) d\mathbf{x} \approx \|\mathbf{x}_{g'}^G - \mathbf{x}_g^G\| (u_{g'}(\tilde{\mathbf{r}}_t) - u_g(\tilde{\mathbf{r}}_t))/2$. This clearly promotes paths through locations with high uncertainty. The trajectory can be recomputed periodically or after reaching each destination. Although the resulting complexity is very low, the limitation is that wiggly trajectories, sometimes preferable [20], are penalized by this criterion.

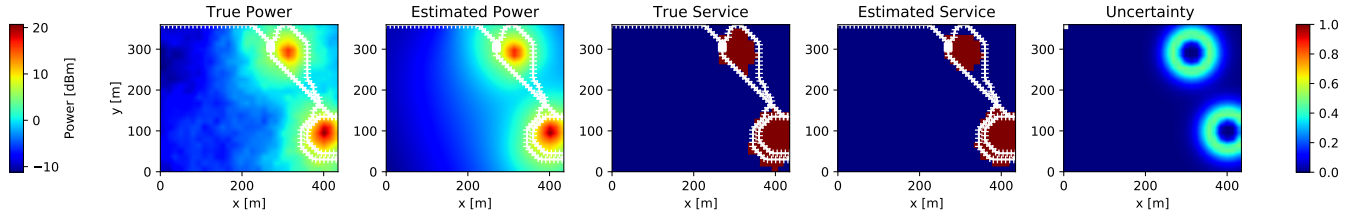


Fig. 1: Trajectory (white line) followed by the autonomous UAV in a sample spectrum surveying operation.

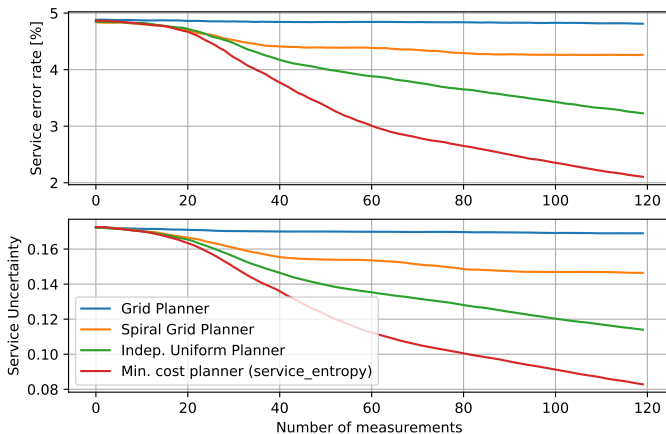


Fig. 2: Comparison between the proposed minimum cost planner and three benchmarks.

4. NUMERICAL EXPERIMENTS

This section assesses the performance of the proposed algorithms by means of simulations. To ensure reproducibility, all the code will be made available at the authors’ websites.

For simplicity, simulations are carried out assuming that the UAV stays at a constant height of 20 m and, therefore, $d = 2$. A 30×25 rectangular grid is constructed over the area of interest with a separation of 10 m between each pair of adjacent grid points. Two transmitters of height 10 m are deployed at locations drawn uniformly at random over \mathcal{X} . The true map is generated by drawing $r^{\mathcal{G}}$ from a Gaussian distribution according to (3), where $l(x)$ is obtained for a path loss exponent of 2, frequency 2.4 GHz, and isotropic transmit antennas. The transmit power is set to $P_{\text{Tx}} = 10$ dBm for both sources. Due to space limitations, we focus on illustrating the effect of shadowing and, thus, σ_w^2 and σ_z^2 are set to 0. The shadowing is generated with $\delta_0 = 50$ m, $\sigma_s^2 = 9$, and $\mu_s = 0$. To generate measurements off the grid, $r^{\mathcal{G}}$ is interpolated using cubic splines. To generate the service map, r_{min} is set to 5 dBm.

The route planning algorithm described at the end of Sec. 3.2 is implemented with a 3×3 kernel of all ones. A trajectory is updated only every time the UAV reaches the destination. This update is performed through the well-known Bellman-Ford algorithm for shortest path. The candidate

waypoints lie on \mathcal{G} and the UAV is allowed to move in one out of 8 directions that differ 45 degrees. The uncertainty of the maps corresponding to each transmitter is aggregated through a max operation; cf. Sec. 3.1. Since there is no algorithm for spectrum surveying in the literature, the proposed method is compared against three benchmarks. Each benchmark corresponds to a different approach to plan the trajectory. The first follows parallel lines, thus having waypoints on a rectangular grid (grid planner); the second follows a rectangular spiral, and the third selects the next destination uniformly at random, then moves there straight ahead. To ensure a fair comparison, all tested approaches collect a measurement every 5 m on their trajectory. This means that, under the assumption of constant speed, the time required to collect t measurements is the same for all approaches. Similarly, all approaches use the proposed online estimator.

Performance is assessed in terms of total uncertainty $u(\tilde{r}_t)$ and the service error rate, which is the fraction of grid points $x_g^{\mathcal{G}}$ where $\beta(x_g^{\mathcal{G}})$ differs from its estimate. Fig. 1 depicts the true and estimated power map, the true and estimated service map, as well as the service uncertainty (cf. (9)) before starting to measure. As observed, the regions with highest uncertainty form rings around the sources (see Sec. 3.1). The trajectory generated by the proposed route planner is observed to target precisely these locations. Fig. 2 compares the reduction of the error rate and uncertainty for the tested algorithms with a Monte Carlo simulation. It is observed that the proposed scheme results in a steeper slope, confirming that it learns the map faster than the benchmarks.

5. CONCLUSIONS

This paper proposes collecting radio measurements with an autonomous UAV to construct radio power and service maps in two steps. First, an online Bayesian learning algorithm obtains the posterior distribution of the radio map at a set of grid locations given all past measurements. This not only provides map estimates but also their associated uncertainty via the posterior variance. Second, a route planner algorithm uses the relevant uncertainty metric to plan a trajectory along areas with high uncertainty, which naturally leads to acquire measurements at approximately the most informative locations.

6. REFERENCES

- [1] S. Grimoud, S. B. Jemaa, B. Sayrac, and E. Moulines, "A REM enabled soft frequency reuse scheme," in *Proc. IEEE Global Commun. Conf.*, Miami, FL, Dec. 2010, pp. 819–823.
- [2] H. B. Yilmaz, T. Tugcu, F. Alagöz, and S. Bayhan, "Radio environment map as enabler for practical cognitive radio networks," *IEEE Commun. Mag.*, vol. 51, no. 12, pp. 162–169, Dec. 2013.
- [3] J. Chen and D. Gesbert, "Optimal positioning of flying relays for wireless networks: A LOS map approach," in *Proc. IEEE Int. Conf. Commun.* IEEE, 2017, pp. 1–6.
- [4] S. Zhang, Y. Zeng, and R. Zhang, "Cellular-enabled UAV communication: A connectivity-constrained trajectory optimization perspective," *IEEE Trans. Commun.*, vol. 67, no. 3, pp. 2580–2604, Mar. 2018.
- [5] A. Alaya-Feki, S. B. Jemaa, B. Sayrac, P. Houze, and E. Moulines, "Informed spectrum usage in cognitive radio networks: Interference cartography," in *Proc. IEEE Int. Symp. Personal, Indoor Mobile Radio Commun.*, Cannes, France, Sep. 2008, pp. 1–5.
- [6] B. A. Jayawickrama, E. Dutkiewicz, I. Oppermann, G. Fang, and J. Ding, "Improved performance of spectrum cartography based on compressive sensing in cognitive radio networks," in *Proc. IEEE Int. Commun. Conf.*, Budapest, Hungary, Jun. 2013, pp. 5657–5661.
- [7] J.-A. Bazerque and G. B. Giannakis, "Distributed spectrum sensing for cognitive radio networks by exploiting sparsity," *IEEE Trans. Signal Process.*, vol. 58, no. 3, pp. 1847–1862, Mar. 2010.
- [8] S.-J. Kim and G. B. Giannakis, "Cognitive radio spectrum prediction using dictionary learning," in *Proc. IEEE Global Commun. Conf.*, Atlanta, GA, Dec. 2013, pp. 3206 – 3211.
- [9] D. Lee, S.-J. Kim, and G. B. Giannakis, "Channel gain cartography for cognitive radios leveraging low rank and sparsity," *IEEE Trans. Wireless Commun.*, vol. 16, no. 9, pp. 5953–5966, Jun. 2017.
- [10] M. Tang, G. Ding, Q. Wu, Z. Xue, and T. A. Tsiftsis, "A joint tensor completion and prediction scheme for multi-dimensional spectrum map construction," *IEEE Access*, vol. 4, pp. 8044–8052, Nov. 2016.
- [11] D.-H. Huang, S.-H. Wu, W.-R. Wu, and P.-H. Wang, "Cooperative radio source positioning and power map reconstruction: A sparse Bayesian learning approach," *IEEE Trans. Veh. Technol.*, vol. 64, no. 6, pp. 2318–2332, Aug. 2014.
- [12] Y. Teganya, D. Romero, L. M. Lopez-Ramos, and B. Beferull-Lozano, "Location-free spectrum cartography," *IEEE Trans. Signal Process.*, vol. 67, no. 15, pp. 4013–4026, Aug. 2019.
- [13] D. Romero, S.-J. Kim, G. B. Giannakis, and R. López-Valcarce, "Learning power spectrum maps from quantized power measurements," *IEEE Trans. Signal Process.*, vol. 65, no. 10, pp. 2547–2560, May 2017.
- [14] D. Romero, Donghoon Lee, and G. B. Giannakis, "Blind radio tomography," *IEEE Trans. Signal Process.*, vol. 66, no. 8, pp. 2055–2069, 2018.
- [15] J.-A. Bazerque, G. Mateos, and G. B. Giannakis, "Group-lasso on splines for spectrum cartography," *IEEE Trans. Signal Process.*, vol. 59, no. 10, pp. 4648–4663, Oct. 2011.
- [16] X. Han, L. Xue, F. Shao, and Y. Xu, "A power spectrum maps estimation algorithm based on generative adversarial networks for underlay cognitive radio networks," *Sensors*, vol. 20, no. 1, pp. 311, Jan. 2020.
- [17] Y. Teganya and D. Romero, "Data-driven spectrum cartography via deep completion autoencoders," in *IEEE Int. Conf. Commun.*, Jun. 2020, *arXiv:1911.12810*.
- [18] J. Chen, U. Yatnalli, and D. Gesbert, "Learning radio maps for UAV-aided wireless networks: A segmented regression approach," in *Proc. IEEE Int. Conf. Commun.*, Paris, France, May 2017, pp. 1–6.
- [19] Y. Zeng, X. Xu, S. Jin, and R. Zhang, "Simultaneous navigation and radio mapping for cellular-connected UAV with deep reinforcement learning," *available at arXiv::2003.07574*, 2020.
- [20] A. Blum, S. Chawla, D. R. Karger, T. Lane, A. Meyerson, and M. Minkoff, "Approximation algorithms for orienteering and discounted-reward TSP," *SIAM J. Comput.*, vol. 37, no. 2, pp. 653–670, Jun. 2007.
- [21] M. Gudmundson, "Correlation model for shadow fading in mobile radio systems," *Electron. Letters*, vol. 27, no. 23, pp. 2145–2146, 1991.
- [22] C. M. Bishop, *Pattern Recognition and Machine Learning*, Information Science and Statistics. Springer, 2006.
- [23] S. M. Kay, *Fundamentals of Statistical Signal Processing, Vol. I: Estimation Theory*, Prentice-Hall, 1993.
- [24] J. Le Ny and G. J. Pappas, "On trajectory optimization for active sensing in gaussian process models," in *Proc. IEEE Conf. Decision Control/Chinese Control Conf.*, Shanghai, China, Dec. 2009, pp. 6286–6292.